3D Respiratory Motion Compensation by Template Propagation

Peter Rösch[1], Thomas Netsch[1], Marcel Quist[2], and Jürgen Weese[1]

[1] Philips Research Laboratories, Sector Technical Systems
Röntgenstraße 24, D-22335 Hamburg, Germany
[2] MIMIT Advanced Development, Philips Medical Systems Nederland B.V.
Veenpluis 4–6, NL-5680 DA Best, The Netherlands

Abstract. A new approach for the automatic estimation of dense 3D deformation fields is proposed. In the first step, template propagation (an advanced block matching strategy) produces not only a large set of point correspondences, but also a quantitative measure of the "registration quality" for each point pair. Subsequently, the deformation field is obtained by a method based on Wendland radial base functions. This method has been adapted to incorporate "registration quality" into regularization, where Morozov's discrepancy principle has been applied to give intuitive meaning to the regularization parameter. The main advantage of the presented algorithm is the ability to perform an elastic registration in the presence of large deformations with minimum user interaction. Applying the method, complicated respiratory motion patterns in 3D MR images of the thorax have been successfully determined. The complete procedure takes less than one hour on a standard PC for MR image pairs (256×256×75 voxels) showing a 40 mm displacement of the diaphragm.

1 Introduction

Respiratory motion often complicates the comparison of images of the thorax, e.g. for the combination of PET and CT images [1] or for cardiac applications [2]. The interpretation of these data sets can be supported by image registration. Registration algorithms aim at finding the transformation that relates the position and orientation of anatomical structures in one image to the pose of the same structures in other images. In order to register images affected by respiratory motion, global rigid or affine transformations are not sufficient as rigid structures, e.g. ribs, move relative to each other and soft tissue is deformed so that non-rigid registration is required. One class of non-rigid registration algorithms incorporate physical tissue properties [3] and often require a model generation step which includes image segmentation and knowledge about tissue elasticity and viscosity. Another class of methods is based on image intensities alone. The majority of current gray value based non-rigid registration algorithms use interpolating base functions to parameterize the non-rigid transformation. An iterative procedure is applied to determine the control point configuration corresponding to optimum similarity between the reference image and the elastically

T. Dohi and R. Kikinis (Eds.): MICCAI 2002, LNCS 2489, pp. 639–646, 2002.
© Springer-Verlag Berlin Heidelberg 2002

transformed target image [1,4,5]. This requires a large number of parameters to be varied for each optimization step. In contrast to these methods, the algorithm described here follows a two-step strategy. First, a local rigid optimization scheme called template propagation [6] that has already been applied in the context of 3D respiratory motion [2] is used. Starting from a single correspondence indicated by the user, this method automatically establishes a large number of correspondences and a quantitative measure of the "registration quality" for each correspondence [8]. In the second step, this information serves as input for an interpolation scheme using radial base functions with compact support presented in [9]. This scheme has been adapted so that the "registration quality" can be incorporated efficiently by regularization. In order to keep the number of parameters small, and to give intuitive meaning to the remaining parameters, automated procedures to adapt the parameters to the properties of the image data have been introduced.

The algorithm is described in the next section. Section 3 is concerned with the application of the algorithm to 3D images of the thorax, and with the discussion of the results. Finally, conclusions are drawn in section 4.

2 Algorithm for 3D Deformation Field Estimation

2.1 Establishing Correspondences by 3D Template Propagation

Template propagation can be classified as an advanced block matching strategy. In contrast to other block matching methods [10], individual blocks (templates) are "aware" of each other. In particular, local rigid transformation parameters obtained for one template serve as starting estimates for the registration of its neighbors. Furthermore, the order in which the individual templates are treated is determined dynamically during registration such that the most "promising" candidate is registered next while outliers are rejected immediately. Template propagation requires a similarity measure like local correlation (LC) [11] that is applicable to small volumes and a method to quantify the "success" of each local registration result. It has been shown that a "quality measure" can be deduced from the properties of the LC optimum and that this measure is closely related to the local registration accuracy [8].

The procedure typically produces several thousand pairs of corresponding points together with the quality measure q for each pair. In order to select a homogeneously distributed subset of correspondences originating from the most successful template registration steps, all templates are discarded for which $q < t \cdot q_{\max}$ holds where $q_{\max}$ is the largest q value found for all template pairs and $0 < t < 1$ is a relative threshold specified by the user. To the remaining templates, a "thinning" procedure is applied such that a set of high quality correspondences with minimum distance d_c between control points in the reference image is obtained where d_c is chosen by the user. The resulting set serves as input to the procedure described in the following section.

2.2 Turning Correspondences into a Dense Deformation Field

The elastic registration scheme used here has been proposed by Fornefett et al. [9]. It is based on the Ψ-functions of Wendland [12]. In contrast to thin plate splines [13], the Wendland functions have compact support which makes sure that changes to the position of a landmark influences the deformation field only in the vicinity of this landmark. For the application presented here, the C^4 continuous $\Psi_{3,2}$ Wendland function has been chosen:

$$\Psi(r) = \Psi_{3,2}(r) = \begin{cases} (1-r)^6 \left(35r^2 + 18r + 3\right) & \text{if } 0 \leq r < 1 \\ 0 & \text{if } r \geq 1 \end{cases} \tag{1}$$

Given a position $\boldsymbol{x}$ in the reference image and a parameter matrix $\boldsymbol{\alpha}$ the transformed position in the target image, $\boldsymbol{y}(\boldsymbol{x})$, is

$$\boldsymbol{y}(\boldsymbol{x}) = \sum_{i=1}^{n} \boldsymbol{\alpha}(\boldsymbol{p}, \boldsymbol{u}, \boldsymbol{a}, \boldsymbol{\lambda})_i \, \Psi(|\boldsymbol{x} - \boldsymbol{p}_i|/a) \tag{2}$$

where $\boldsymbol{p}_i$ and $\boldsymbol{u}_i$ are the positions of n corresponding landmarks in the reference and target image, respectively. The support length a could be set by an expert user who can estimate the degree of deformation in the images under consideration and thus select a value for a that is large enough to avoid folding, but small enough to describe local deformations. Fortunately, the minimum value for a that guarantees preservation of topology for isolated landmarks can be determined analytically [9] as $a = 4.33\Delta$ in 3D where Δ is the landmark displacement. This allows for an automatic calculation of a by determining the maximum of Δ for all control point pairs.

The parameter matrix $\boldsymbol{\alpha}$ in (2) is obtained by solving

$$\left(\boldsymbol{K} + \lambda \boldsymbol{W}^{-1}\right) \boldsymbol{\alpha} = \boldsymbol{u}, \; K_{i,j} = \Psi\left(|\boldsymbol{p}_i - \boldsymbol{u}_j|/a\right), \; \boldsymbol{W} = \operatorname{diag}\{w_1 \ldots w_n\} \tag{3}$$

For Wendland functions and non-coplanar sets of 3D landmarks, it has been proven that (3) has a unique solution [12]. Setting the regularization parameter λ to zero corresponds to interpolation, i.e. $\boldsymbol{y}(\boldsymbol{p_i}) = \boldsymbol{u}_i$, whereas $\boldsymbol{\alpha}$ parameterizes a global affine transformation for $\lambda \to \infty$. If the correspondences have been obtained by template propagation, the weights of the individual landmarks can be set to $w_i = q_i$ so that correspondences originating from accurate template matching steps contribute most to the deformation field.

It is well known from the theory of ill-posed problems that λ often lacks intuitive meaning. An approach to relate λ to the localization errors σ_i of landmarks is Morozov's discrepancy principle [14]. This principle can be applied here by determining the value of λ that results in a certain average deviation $\overline{\sigma}$ of landmark positions $\boldsymbol{u}_i$ in the target image from the positions obtained by transforming the corresponding source landmarks, $\boldsymbol{y}(\boldsymbol{p}_i)$, where $\overline{\sigma}$ should be of the same order as the landmark localization error. As $\overline{\sigma}$ increases monotonically with λ, the resulting equation (4) can be efficiently solved for λ with the Newton method.

$$\left(\sum_{i=1}^{n} q_i\right)^{-1} \sum_{i=1}^{n} q_i \left(\boldsymbol{u}_i - \sum_{k=1}^{n} \boldsymbol{\alpha}(\boldsymbol{p}, \boldsymbol{u}, a, \lambda)_k \, \Psi(|\boldsymbol{p}_i - \boldsymbol{p}_k|/a)\right)^2 = \overline{\sigma}^2 \tag{4}$$

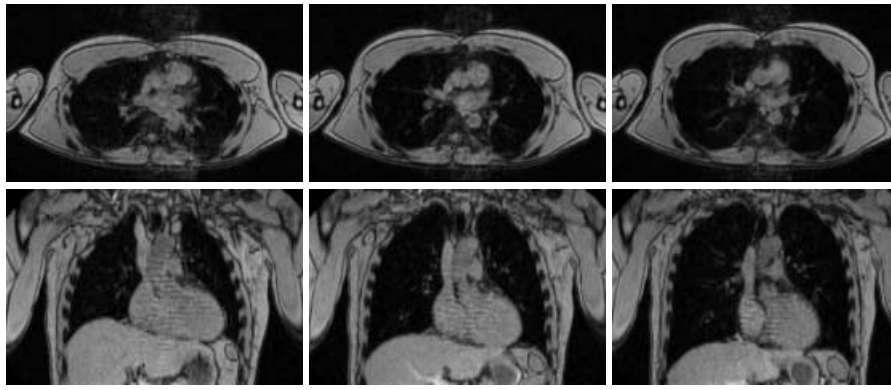

Fig. 1. Axial (top), coronal (bottom) slices of 3D MR images of the human thorax. Images have been taken in three respiratory states: "exhale" (left), "intermediate" (center) and "inhale" (right). The image sizes are 256×256×75 voxels with a voxel size of 1.76×1.76×4 mm^3.

3 Experiments and Results

3.1 Images Used for the Experiments

Three 3D MR images of a volunteer showing the thorax and parts of the abdomen at different diaphragm positions have been acquired using a multi slice FFE sequence. The sequence allowed 75 axial slices to be acquired during a single breathhold. Orthogonal slices of the images are shown in fig. 1. A diaphragm shift of about 40 mm between the images corresponding to "inhale" and "exhale" has been observed. As the focus of this investigation was the motion of the chest and the pulmonary vessels, image acquisition has not been ECG-triggered so that motion blurring occurred in the vicinity of the heart.

3.2 Experimental Setup and Parameters

The algorithm requires approximate local registration parameters at one or more image locations for the initialization of template propagation. This information has been obtained by interactively indicating the location of one anatomical structure in all images to be registered. In this case, the position where the pars scapularis joins the m. lattisimus dorsi is clearly visible in all images (see fig. 2). An estimate of the local translation parameter at this position is given directly by the coordinate differences. Since the orientation of the chosen structure is almost the same in all three images, and the algorithm only requires approximate starting estimates, rotation angles of zero could be used as initial estimates. As the slice thickness in the present case is relatively large, and in order to make sure that templates contain sufficient structure in image regions with little contrast, the template size has been set to 20 mm which is in the upper range of

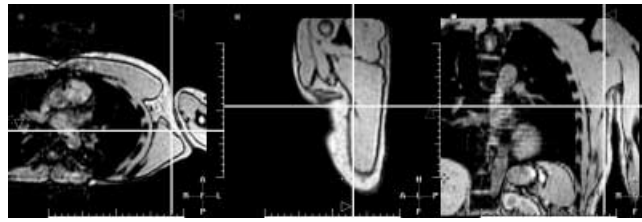

Fig. 2. Single correspondence used for the initialization of template propagation. As it was visible in all data sets, the position where the pars scapularis joins m. latissimus dorsi indicated by the white cross hair has been chosen manually.

values used previously [6,8]. An overlap between neighboring templates has been allowed, since this results in a higher robustness compared to non-overlapping templates in the presence of large deformations [6]. In order to include templates in image areas with poor signal to noise ration (e.g. the lung) the relative "quality threshold" (see section 2.1) has been set to $t = 0.2$. The minimum distance between control points in the reference image has been set to $d_c = 20$ mm. Two values for $\overline{\sigma}$ (see section 2.2), $\overline{\sigma} = 0$ and $\overline{\sigma} = 1$ mm have been used. The first setting results in an interpolating deformation field and the second value corresponds to the typical localization error for successfully registered templates found experimentally [8].

3.3 Discussion of Experimental Results

Using the parameter settings given above, the first experiment was concerned with estimating the deformation field between the "inhale" and "intermediate" image. The even more challenging task of elastically matching the "inhale" to the "exhale" image using interpolating and approximating deformation fields has been addressed in the second and third experiment.

In order to characterize the results, the deformation fields have been used to reformat one of the images. Afterwards, gray value differences between the reference and reformatted target images are assessed visually. As all images have been acquired within a couple of minutes using the same protocol, contrast variations between images are small and the gray values of the difference image are closely related to the local registration accuracy. The plausibility of the results has been illustrated by applying the deformation field to a regular grid which is then overlaid on the target image. Results are shown in figures 3 and 4.

In all experiments, about 15000 templates have been selected and registered from which about 1100 correspondences have been used for the estimation of the deformation field. Support lengths of $a = 79$ mm and $a = 192$ mm have been determined automatically for the first and second/third experiment, respectively. The smaller value for the first experiment reflects the smaller degree of deformation between the "intermediate" and "inhale" image.

For all experiments, the differences of the unregistered images show a significant amount of residual structures resulting from chest expansion. Furthermore,

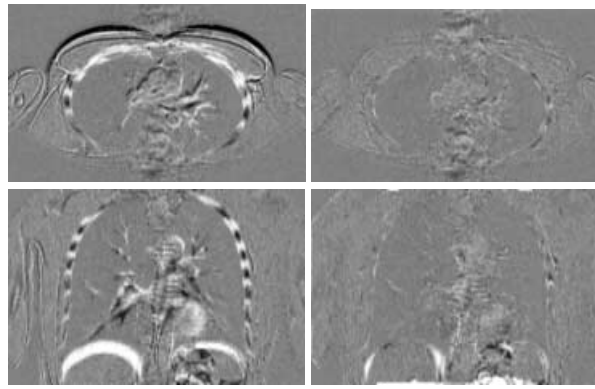

Fig. 3. Difference images between "inhale" and "intermediate" state before (left) and after (right) elastic registration with $\overline{\sigma} = 0$.

motion of pulmonary vessels and the diaphragm affect the difference images. After registration using interpolating deformation fields in the first and second experiment, the presence of residual structures is reduced considerably, particularly in the chest area including the pulmonary vessels (see right column of fig. 3 and center column of fig. 4) indicating successful registration. However, inaccuracies show up close to the diaphragm and in the second experiment, close to the ribs.

The main reason for the inaccuracies close to the ribs in the second experiment is that the deformation field is based on about 1000 correspondences in all cases although larger deformations need to be treated compared to the first experiment. Using a smaller value of d_c and thus a larger number of corresponding points would lead to a more accurate deformation field at the cost of higher computation time. A second complication in the presence of larger deformations is that the contents of the individual templates are more strongly deformed which results in larger local registration inaccuracies. In particular, if an interpolating deformation field is estimated all correspondences are weighted equally and the incorporation of "low quality" templates degrades the result.

This problem can at least partially be solved by weighting the contribution of the individual template pairs by their "registration quality" in the context of regularization (see section 2.2) as could be demonstrated in the third experiment. The right column of fig. 4 indicates that residual structures close to the ribs could be reduced by using approximation rather than interpolation. The deformation grid given at the bottom of fig. 4 reflects the expansion of the chest and shows that the mediastinum, and the heart, to some extent follow the motion of the diaphragm.

In all experiments, the most striking structures in the difference images are located in the abdomen close to the diaphragm where internal structures e.g. of the liver are hardly visible in the images used here so that few reliable correspondences could be established in this area.

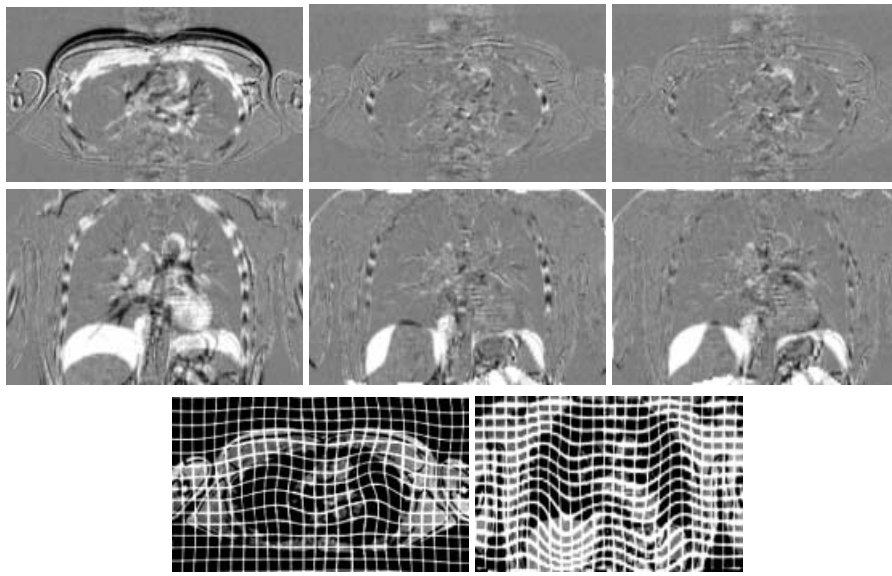

Fig. 4. Axial and coronal slices of 3D difference images "exhale"-"inhale" before (left) and after elastic registration using $\overline{\sigma} = 0$ (center) and $\overline{\sigma} = 1$ mm (right). At the bottom, the deformation grid obtained for $\overline{\sigma} = 1$ mm is visualized.

Calculation times for the complete procedure including template propagation, deformation field estimation and the application of the deformation field were 32, 38 and 51 minutes on a 1.7 GHz P4 PC with 1 GB of memory for the first, second and third experiment, respectively. Compared to the first experiment, the larger support length led to a larger number of non-zero contributions in (2) and thus to an increase of calculation time in the second case. In the third experiment, a Newton optimization to find $\lambda = 0.005$ according to (4) had to be performed additionally, further increasing the computational cost.

4 Conclusions

An elastic transformation based on Wendland functions [9] has been combined with the template propagation algorithm originally described in [6]. The particular advantage of this combination is that in addition to a set of corresponding points, a quantitative measure of confidence for each point pair is taken into account for the estimation of a dense deformation field. This measure which is closely related to the local registration accuracy [8] is incorporated by regularization which is controlled by a parameter with intuitive meaning. Furthermore, the only user interaction required is the identification of a single point correspondence. The algorithm is capable of estimating accurate 3D deformation fields in the presence of large deformations without prior segmentation of the images, which has been demonstrated by successfully registering 3D MR images

of the chest taken at different instants of the respiratory cycle with diaphragm displacements up to 40 mm. Particularly for large deformations, the optional regularization step further improved the accuracy of the deformation field. Calculation times for the whole procedure were below one hour on a standard PC.

Acknowledgments

The authors would like to thank the image processing group at the Guy's, King's and St Thomas' School of Medicine, London, the participants of the IMAGINE project at the Fachbereich Informatik, Universität Hamburg, and Frans A. Gerritsen, MIMIT Advanced Development for helpful discussions. We also thank our colleagues Dirk Manke and Kay Nehrke for the acquisition of the images.

References

1. D. Mattes, D. Haynor, H. Vesselle, K. Lewellen, W. Eubank: Nonrigid multimodality image registration. Proc. of SPIE **4322** (2001) 1609–1620
2. D. Manke, K. Nehrke, P. Rösch, P. Börnert, O. Dössel: Study of Respiratory Motion in Coronary MRA. Proceedings of ISMRM'01 Elsevier (2001) 1852
3. Rabbitt, R. D., Weiss, J. A., Christensen, G. E., Miller, M. I.: Mapping of hyperelastic deformable templates using the finite element method, Proc. of SPIE **2573** (1995) 252–265
4. Rueckert, D. Sonoda, L.I., Hayes, C., Hill, D. L. G., Leach, M. O., Hawkes, D. J.: Nonrigid registration using free-form deformations: Application to Breast MR images, IEEE Trans Medical Imaging **18** (1999) 712–721
5. G. K. Rohde, A. A. Aldroubi, B. M. Dawant: Adaptive free-form deformation for inter-patient medical image registration. Proc. of SPIE **4322** (2001) 1578–1587
6. P. Rösch, T. Netsch, M. Quist, G. P. Penney, D. L. G. Hill, and J. Weese: Robust 3D deformation field estimation by template propagation. MICCAI 2000, Lecture Notes in Computer Science **1935** (2000) 521–530
7. Little, J. A., Hill, D. L. G., Hawkes, D. J.: Deformations incorporating rigid structures. Computer Vision and Image Understanding **66** (1997) 223–232
8. P. Rösch, T. Mohs, T. Netsch, M. Quist, G. P. Penney, D. J. Hawkes, J. Weese: Template selection and rejection for robust non-rigid 3D registration in the presence of large deformations. SPIE proceedings **4322** (2001) 545–556.
9. M. Fornefett, K. Rohr, and S. Stiehl: Radial base functions with compact support for elastic registration of medical images. Image and Vision Comp. **19** (2001) 87–96
10. Kostelec, P. J., Weaver, J. B., Healy, D. M. Jr.: Multiresolution elastic image registration, Med. Phys. **25** (1998) 1593-1604
11. P. Rösch, T. Blaffert, J. Weese: Multi-modality registration using local correlation, in: H. U. Lemke, M. W. Vannier, K. Inamura, A. G. Farman (Eds) CARS'99 Proceedings, Elsevier (1999) 228–232
12. H. Wendland: Piecewise polynomial, positive definite and compactly supported radial functions of minimal degree. Advances in Computational Mathematics **4** (1995) 389–396
13. Bookstein, F. L.: Principal warps: Thin-plate splines and the decomposition of deformations, IEEE Trans. Patt. Anal. Mach. Intell **11** (1989) 567–585
14. V. A. Morozov: Methods for solving incorrectly posed problems, Springer (1984)